

# Effect of Proton Irradiation on Zr/Nb Nanoscale Multilayer Structure and Properties

Roman Laptev <sup>1,\*</sup>, Dmitriy Krotkevich <sup>1</sup>, Anton Lomygin <sup>1</sup>, Ekaterina Stepanova <sup>1</sup>, Natalia Pushilina <sup>1</sup>, Egor Kashkarov <sup>1</sup>, Aleksandr Doroshkevich <sup>2</sup>, Alexey Sidorin <sup>2</sup>, Oleg Orlov <sup>2</sup> and Vladimir Uglov <sup>3</sup>

<sup>1</sup> Division for Experimental Physics, National Research Tomsk Polytechnic University, Tomsk 634050, Russia; dgk7@tpu.ru (D.K.); adl4@tpu.ru (A.L.); enstepanova@tpu.ru (E.S.); pushilina@tpu.ru (N.P.); ebk@tpu.ru (E.K.)

<sup>2</sup> Joint Institute for Nuclear Research, Dubna 141980, Russia; sidorina@jinr.ru (A.S.); orlov@jinr.ru (O.O.)

<sup>3</sup> Department of Solid State Physics, Belarusian State University, 220006 Minsk, Belarus; uglov@bsu.by

\* Correspondence: laptevrs@tpu.ru; Tel.: +7-913-852-3733

**Abstract:** The effect of proton irradiation on the structure, phase composition, defect state and nanohardness of Zr/Nb nanoscale multilayer coatings was investigated. Preservation of the Zr/Nb layered structure with 50 and 100 nm thick layers, was observed after irradiation with protons at 1720 keV energy and  $3.4 \times 10^{15}$ ,  $8.6 \times 10^{15}$  and  $3.4 \times 10^{16}$  ions/cm<sup>2</sup> fluences, and the interfaces remained incoherent. In the Zr/Nb nanoscale multilayer coatings with individual layer thicknesses of 10 and 25 nm, there were insignificant fluctuations in interplanar distance, which were influenced by changes in irradiation fluence, and the interfaces were partially destroyed and became semicoherent. Changing irradiation fluence in the investigated ranges led to a decrease in the nanohardness of the Zr/Nb nanoscale multilayer coatings with individual layer thicknesses of 10–50 nm. Variable-energy positron Doppler broadening analysis revealed that these changes are primarily caused by peculiarities of the localization and accumulation of the embedded ions and do not cause a significant increase in the S-parameters of Zr/Nb nanoscale multilayer coatings with a layer thickness less than 100 nm.

**Keywords:** nanoscale multilayer coatings; proton irradiation; microstructure; positron annihilation; radiation defects; nanohardness



**Citation:** Laptev, R.; Krotkevich, D.; Lomygin, A.; Stepanova, E.; Pushilina, N.; Kashkarov, E.; Doroshkevich, A.; Sidorin, A.; Orlov, O.; Uglov, V. Effect of Proton Irradiation on Zr/Nb Nanoscale Multilayer Structure and Properties. *Metals* **2023**, *13*, 903. <https://doi.org/10.3390/met13050903>

Academic Editors: Jie Hou and Xiao Zhou

Received: 13 April 2023

Revised: 29 April 2023

Accepted: 5 May 2023

Published: 6 May 2023



**Copyright:** © 2023 by the authors. Licensee MDPI, Basel, Switzerland. This article is an open access article distributed under the terms and conditions of the Creative Commons Attribution (CC BY) license (<https://creativecommons.org/licenses/by/4.0/>).

## 1. Introduction

A central problem in modern materials science is the development of the scientific basis for advanced technologies for the production of structural materials that are suitable for operation in aggressive conditions with high tolerance. It is well known that damage caused by radiation and hydrogen is one of the most essential factors limiting the service life of most structural materials operating under extremely difficult conditions. The issue of improving tolerance to radiation and hydrogen is still relevant despite the long history of the problem. The creation of functionally graded materials (FGMs) is one of the promising directions for the development of radiation- and hydrogen-tolerant materials with enhanced physical and mechanical properties. FGMs are single-phase or composite materials in which the composition or microstructure changes uniformly or discontinuously to provide different local properties in at least one direction [1,2]. In the case of FGMs, high resistance can be achieved by creating specific defects of different dimensions, resulting in sink formation and high diffusion mobility. In addition, management of the structure and the complex defects makes possible the creation of conditions whereby new defects are annihilated, during operation or temperature rise, due to mobility enhancement. One of the most developed methods of FGM manufacturing is additive manufacturing and physical deposition methods, which allows the fabrication of three-dimensional and two-dimensional FGMs [2]. Recently, the issues surrounding the improvement of the physical

and mechanical properties of FGMs, including the radiation and hydrogen resistance, have been widely investigated [3–8]. The nanoscale multilayer metal systems that are obtained by physical deposition methods are also being actively studied. A considerable number of theoretical and experimental studies of nanoscale multilayer coatings (NMCs), including Zr/Nb based systems, have been performed in recent years [7–10]. Zr/Nb NMCs have several advantages over other incoherent and semicoherent systems: Zr and Nb are nuclear reactor core structural materials with sufficiently high melting point, corrosion resistance and strength, and low thermal neutron cross section, making these FGMs promising for the creation of composite materials for nuclear applications. Proton irradiation of the outer and inner regions of Zr/Nb multilayers shows them to have high radiation tolerance, due to radiation defect sinking at the interfaces with subsequent annihilation [11–14]. At the same time, despite the higher defect sinking capability, the interfaces of thinner layers show a tendency towards microstructural degradation. Additionally, protons also accumulate irregularly at the interfaces, leading to the creation of a significant concentration gradient. This creates the potential for interface degradation and coherence change as the radiation fluence is increased. The aim of this work is to study the fluence effect of proton irradiation on the microstructure, defects and properties of Zr/Nb NMCs with different layer thicknesses to develop a scientific basis for the design of hydrogen and radiation damage-tolerant FGMs.

## 2. Materials and Methods

At the Weinberg Research Center of the National Research Tomsk Polytechnic University (TPU, Tomsk, Russia), the nanoscale multilayer coatings (NMCs) with alternate layers of Zr and Nb were produced using magnetron sputtering. The substrate was a silicon single crystal with the (111) orientation. Before the deposition of multilayer coatings, argon ions were used to clean the substrate (ion current 2.5 mA, voltage 2.5 kV, time 0.5 h, residual pressure in the chamber 2 mPa). The multilayers were deposited using a magnetron sputtering system with two independent targets made of pure niobium and zirconium. Prior to deposition, the vacuum chamber was evacuated to a residual pressure of 0.005 Pa. The deposition of multilayers was carried out in an argon atmosphere (operating pressure 0.3 Pa). As a result, Zr/Nb NMCs with individual layer thicknesses of 10, 25, 50 and 100 nm were obtained (hereinafter these samples will be designated as Zr10/Nb10, Zr25/Nb25, Zr50/Nb50 and Zr100/Nb100, respectively). The total thickness of all produced Zr/Nb coatings was in the range 0.9–1.3  $\mu\text{m}$ .

Irradiation of obtained Zr/Nb NMCs by a perpendicular proton beam (energy 1720 keV) was performed through a 33  $\mu\text{m}$  aluminum degrader in the EG-5 electrostatic Van de Graaff accelerator at the Neutron Physics Laboratory (Joint Institute for Nuclear Research, Dubna, Russia). The corresponding Bragg peaks were located at  $85 \pm 30$  nm. The fluences were  $3.4 \times 10^{15}$ ,  $8.6 \times 10^{15}$  and  $3.4 \times 10^{16}$  ions/cm<sup>2</sup> according to the irradiation parameters.

Among the various research methods, it is worth noting the positron annihilation spectroscopy (PAS) methods that are prospective methods for analyzing the defect structure of FGMs during irradiation and hydrogen accumulation. This allows the investigation of the mechanisms and control of the kinetics of the appearance, transformation and dissipation of different dimensional defects at a wide range of concentrations. Doppler broadening spectroscopy (DBS), with the variable positron energy beam at the Dzheleпов Laboratory of Nuclear Problems (Joint Institute for Nuclear Research, Dubna, Russia), was used to investigate the defect structure. We used a monoenergetic positron beam (spot diameter 5 mm and intensity  $10^6$  e<sup>+</sup>/s). The energy of the implanted positrons varied in the range 0.1–30 keV. An HPGe detector model GEM25P4-70 (AMETEK ORTEC, Oak Ridge, TN, USA), with an energy resolution of 1.20 keV interpolated for the energy of 511 keV, was used for the Doppler broadening measurements. The obtained DBS spectra were analyzed by extracting the S and W parameters. Parameter S is defined as the ratio between the number of positron annihilation events in the central part of the annihilation peak and the total number of events below this peak. This parameter characterizes the positron

annihilation probability with low-momentum electrons. The  $W$  parameter is defined as the ratio of the number of positron annihilation events in the wings of the annihilation peak to the total peak area. This parameter characterizes the annihilation probabilities of positrons with semi-core and core electrons and is sensitive to changes in the chemical environment at the annihilation site.

Glow discharge optical emission spectrometry (GD-OES) was used to study the layer-by-layer distribution of Zr, Nb and H (GD-Profilier 2 spectrometer, Horiba Scientific, Palaiseau, France). The Zr/Nb NMCs study was performed using a radio-frequency source under the following conditions: 650 Pa of pressure, 40 W of power, 1 kHz of frequency and 25% of duty cycle. The obtained spectra were corrected by exponential dependence approximation [15].

For microstructural characterization, methods of transmission electron microscopy (TEM) were used (JEM-2100F electron microscope, JEOL, Akishima, Japan). Thin foils for electron microscopy were produced by Ion Slicer EM-09100IS (JEOL, Akishima, Japan) (etching angle was  $1.5\text{--}4^\circ$  and acceleration voltage was 8 kV). XRD analysis was used to determine the phase composition with an XRD-7000S diffractometer (Shimadzu, Japan) ( $2\theta$  varied in the range  $20\text{--}75^\circ$  with a scanning rate of  $5.0\text{ deg/min}$ ). The nanohardness was evaluated with the use of a Table Top Nanoindentation System (CSM Instruments, Peseux, Switzerland). Measurement of at least 20 indentations was carried out at a load of 5 mN and an exposure time of 30 s.

### 3. Results

The depth profiles of DBS parameters in Zr/Nb nanoscale multilayer coatings NMCs with different individual layer thicknesses as a function of proton irradiation fluence are presented in Figure 1.

For Zr10/Nb10 samples, there is no substantial change in the annihilation parameters when the fluence of proton irradiation is increased. The values of the  $S$  and  $W$  parameters in the proton deposition area ( $85 \pm 30\text{ nm}$ ) before and after irradiation are preserved even at a fluence of  $3.4 \times 10^{16}\text{ ions/cm}^2$ . The  $S(E)$  and  $W(E)$  profiles have a typical pattern due to the presence of reduced electron density at the interfaces on the zirconium side and its high affinity, which determines the favorable positron localization in the zirconium vicinity at positron energies greater than 0.1 keV [11,12]. A significant growth in the  $S$ -parameter and a reduction in the  $W$ -parameter, which would indicate an intense defect accumulation, also does not occur as a result of increasing the proton irradiation fluence for the Zr/Nb NMCs with an individual layer thickness of 25 nm. The changes in the DBS parameters are mainly in the experimental error, but a slight increase in the  $S$ -parameter values at positron energies above 14 keV is observed during irradiation with a maximum fluence  $3.4 \times 10^{16}\text{ ions/cm}^2$ . Slight differences in the  $S(E)$  and  $W(E)$  profiles of Zr10/Nb10 and Zr25/Nb25 before and after irradiation are probably due to the different number of interfaces and related morphological characteristics.

With positron beam energies greater than 11 keV, Zr50/Nb50 exhibits a significant decrease in the  $S$ -parameter values (and an increase in the  $W$ -parameter values). Typically, such dependencies ( $S \downarrow, W \uparrow$ ) are observed when the free volume decreases as a result of defect annealing [16] or hydrogen accumulation [17]. All post-irradiation values are almost within the boundaries of experimental error, and there are no significant changes as a result of increasing proton irradiation fluence. Similar changes are observed in Zr100/Nb100 at different proton irradiation fluences, but, in contrast to the 50 nm system, the most significant variations occur in the positron energy range from 1 to 22 keV ( $\sim 10\text{--}650\text{ nm}$ ).

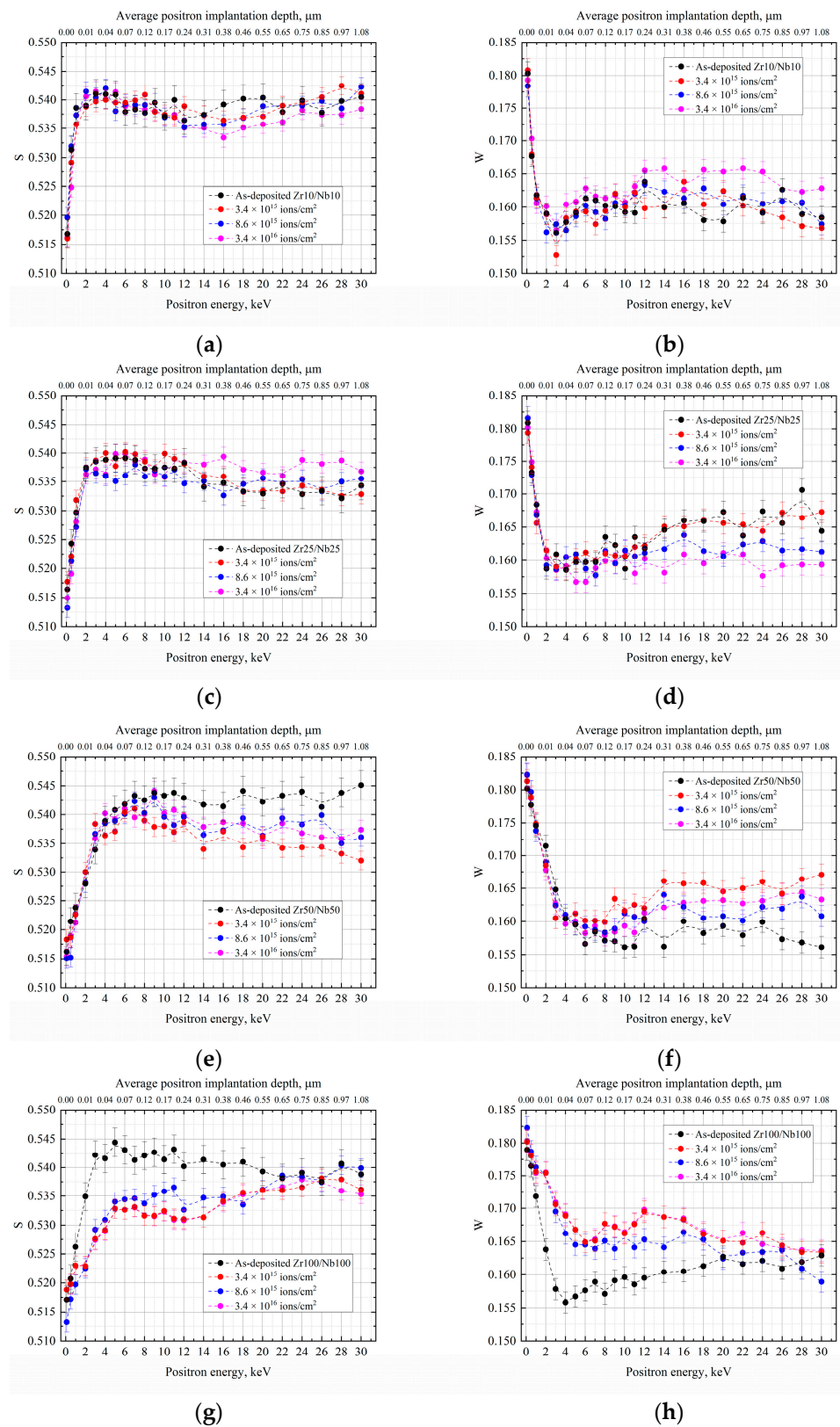


**Figure 1.** The depth profile of DBS parameters in as-deposited and proton-irradiated Zr/Nb nanoscale multilayer coatings (NMCs) with different individual layers thicknesses as a function of proton irradiation fluence:  $S(E)$  (a,c,e,g) and  $W(E)$  (b,d,f,h).

The reasons for these changes can be clarified using the dependence,  $S = f(W)$ , since both indicated parameters depend on the number and type of the positron trapping

centers [18]. If the experimental values of the  $S$  and  $W$  parameters for the dataset are on a straight line, the dominant positron trapping center is considered to be similar. A change in the slope of the straight dependence,  $S = f(W)$ , indicates a change in the dominant positron straight center. The  $S = f(W)$  plot for as-deposited and proton-irradiated Zr/Nb NMCs with different individual layers thicknesses is presented in Figure 2.

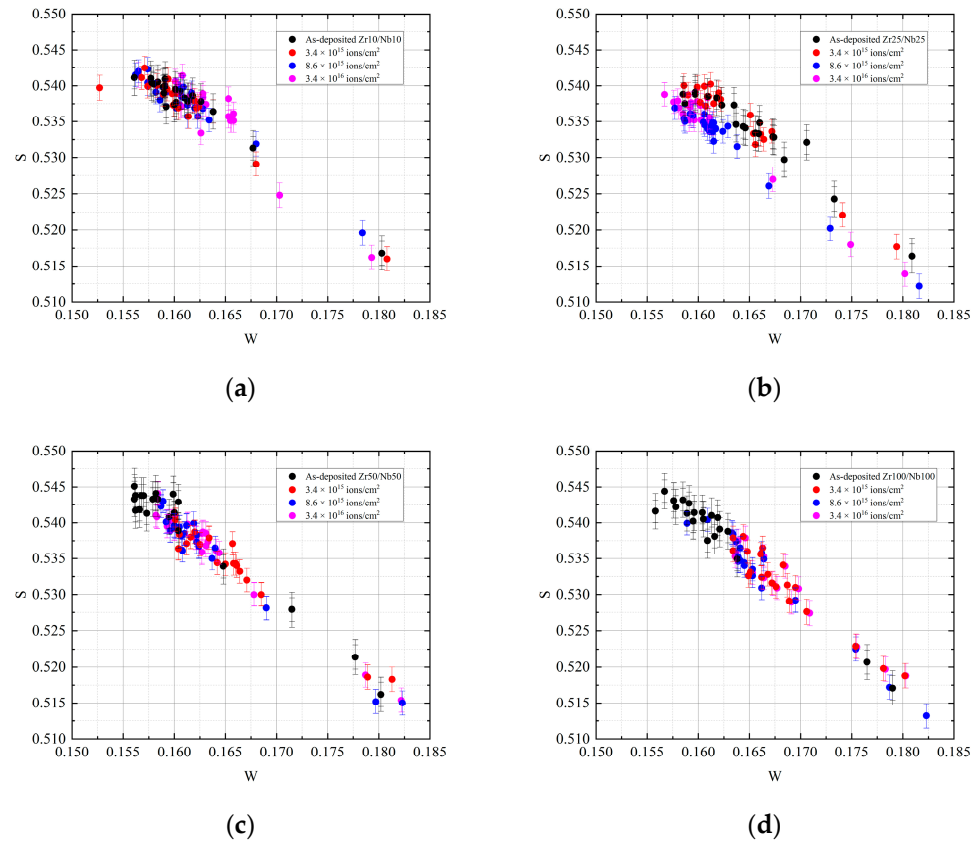


**Figure 2.** The  $S = f(W)$  plot for as-deposited and proton-irradiated Zr10/Nb10 (a), Zr25/Nb25 (b), Zr50/Nb50 (c) and Zr100/Nb100 (d) samples.

The analysis of the dependence,  $S = f(W)$ , shows the preservation of a predominant defect type before and after proton irradiation, regardless of fluence. The scatter of the experimental values of the linear dependence increases for systems with thin individual layers (10 and 25 nm), mainly due to peculiarities of positron annihilation in small size crystallites comparable to the diffusion length. Thus, before and after proton irradiation, regardless of fluence, positrons annihilate mainly in the regions of reduced electron density at the interfaces. However, proton accumulation in these areas can cause its evolution, as is probably observable on the  $S(E)$  and  $W(E)$  profiles for proton irradiated Zr/Nb NMCs with different individual layers thicknesses (Figure 1). The depth of the H profiles of Zr/Nb NMCs with different individual layers thicknesses as a function of proton irradiation fluence are presented in Figure 3.

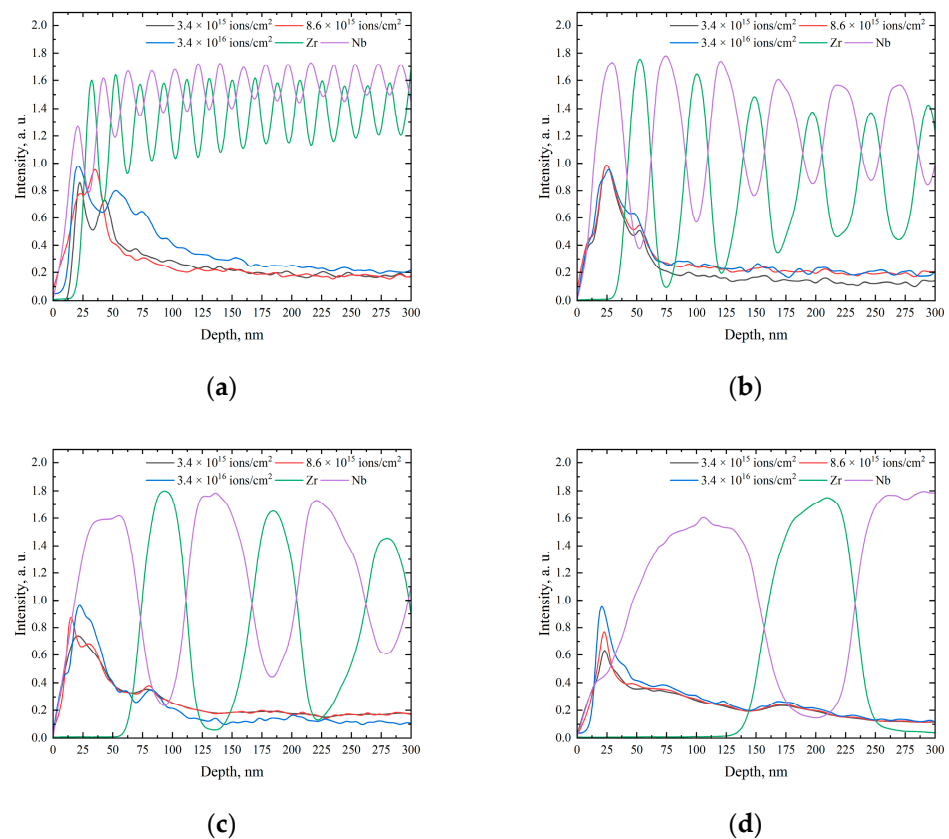


**Figure 3.** The depth profile of hydrogen in proton-irradiated Zr10/Nb10 (a), Zr25/Nb25 (b), Zr50/Nb50 (c) and Zr100/Nb100 (d) samples. The H signal base level in Zr/Nb NMC before proton irradiation is equal to  $0.16 \pm 0.05$  a.u.

After proton irradiation, irregular proton accumulation is also seen at the interfaces in Zr/Nb NMCs [11]. This irregularity is mainly explained by two factors: the fast hydrogen diffusion in the Nb layers (leading to the migration of hydrogen atoms from the layers to the interface where they are trapped and distributed along the interface) and the low hydrogen diffusion in the Zr layers (resulting in hydrogen distribution in the Zr layers according to the Bragg peak). Meanwhile, Zr10/Nb10 samples show a more intensive H signal at depth of 50–130 nm at the maximum irradiation fluence ( $3.4 \times 10^{16}$  ions/cm<sup>2</sup>), probably indicating a partial destruction of the interface structure.

The deposition modes indicated above resulted in formation of Zr/Nb NMCs with alternating zirconium and niobium layers with clearly distinguishable boundaries between individual layers. The microstructures of the as-deposited Zr25/Nb25 and Zr100/Nb100 have previously been described in detail in [11,12]. It was found that the thicknesses of the alternating layers were  $(10 \pm 3)$ ,  $(25 \pm 5)$ ,  $(50 \pm 15)$  and  $(100 \pm 20)$  nm for Zr10/Nb10, Zr25/Nb25, Zr50/Nb50 and Zr100/Nb100, respectively. In all studied NMCs, nanoscale columnar grains with sizes of 10–50 nm, comparable with the layer thickness, are observed in the bulk of the Nb and Zr layers. Thus, the grain sizes for Zr10/Nb10, Zr25/Nb25, Zr50/Nb50 and Zr100/Nb100 are within 5–10 nm, 15–25 nm, 20–50 nm and 20–50 nm, respectively. The presence of a columnar structure is typical for coatings grown under conditions of low-energy ion bombardment and under conditions of limited atomic mobility. The grains in the layers grow perpendicular to the substrate. In addition, Zr/Nb samples with a layer thickness of 10 nm are characterized by the presence of small deformations and distortions of the layers in the near-surface regions. According to TEM studies of cross sections of the obtained Zr/Nb NMCs, the presence of reflections from different planes of the alpha zirconium phase and beta niobium phase is typical for electron microdiffraction from a selected area (SAED) for all the studied samples.

The high-resolution (HR) TEM studies showed the preservation of the multilayer structure for all Zr/Nb samples after proton exposure (Figure 4). After proton irradiation at an energy of 1720 keV and fluences of  $3.4 \times 10^{15}$ ,  $8.6 \times 10^{15}$  and  $3.4 \times 10^{16}$  ions/cm<sup>2</sup>, the Zr/Nb layered structures are preserved for samples with a thickness of 25, 50 and 100 nm. For the Zr50/Nb50 and Zr100/Nb100 samples, the Zr/Nb layer boundary is incoherent. For the Zr10/Nb10 samples, it was not always possible to separate the layers. These samples, after irradiation with protons, are characterized by the presence of nanovoids consisting of several vacant atomic positions. This is especially pronounced for samples after irradiation with the maximum fluence ( $3.4 \times 10^{16}$  ions/cm<sup>2</sup>). After irradiation with protons, the layer boundaries in the Zr10/Nb10 and Zr25/Nb25 samples are semicoherent.

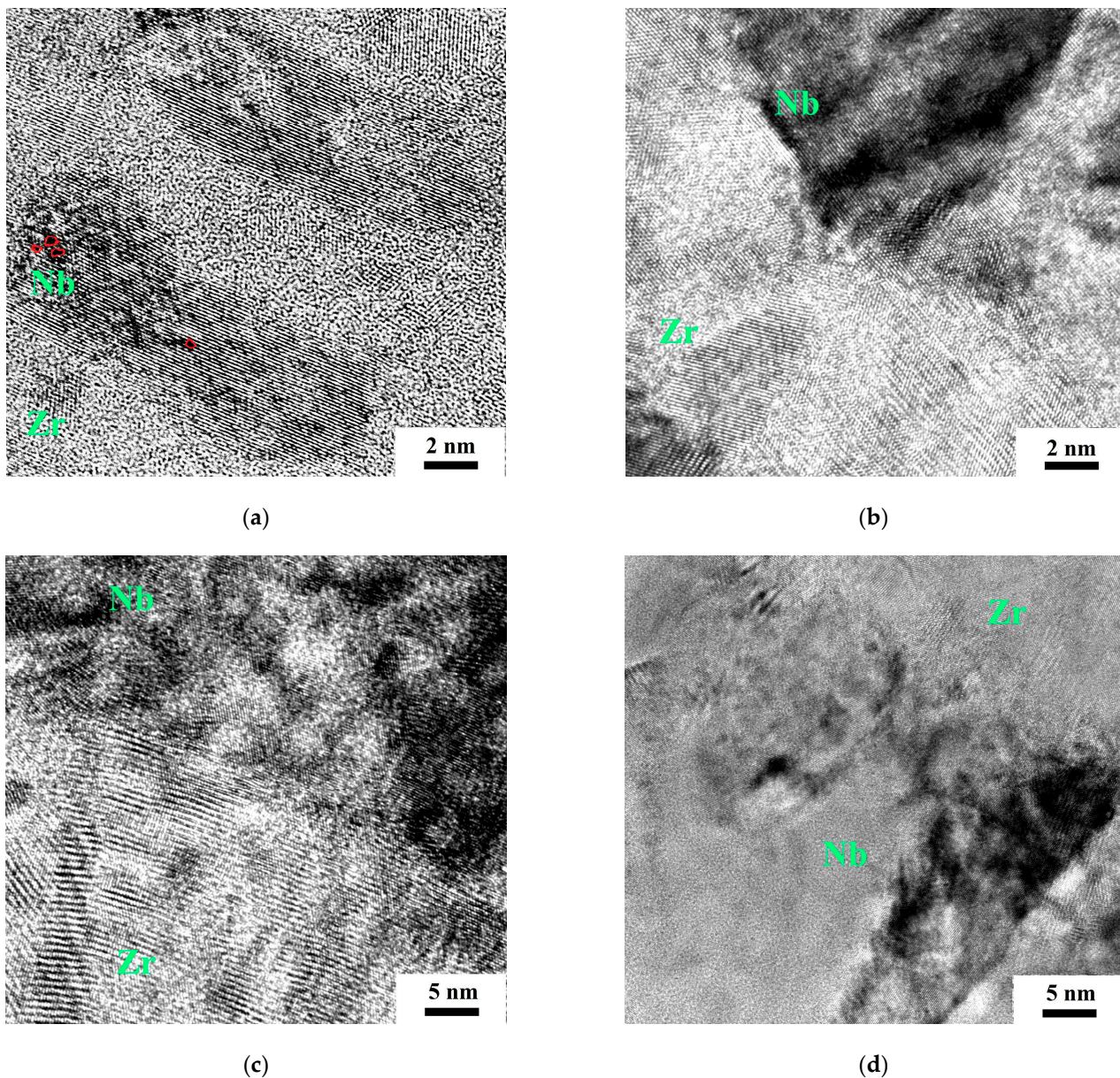


**Figure 4.** HR TEM images of the microstructure cross section of the Zr/Nb samples after proton exposure ( $3.4 \times 10^{16}$  ions/cm<sup>2</sup> fluence) Zr10/Nb10 (a), Zr25/Nb25 (b), Zr50/Nb50 (c) and Zr100/Nb100 (d) samples. The nanovoids are highlighted in red.

Figure 5 shows the XRD diffraction patterns of as-deposited and proton-exposed Zr/Nb NMCs.

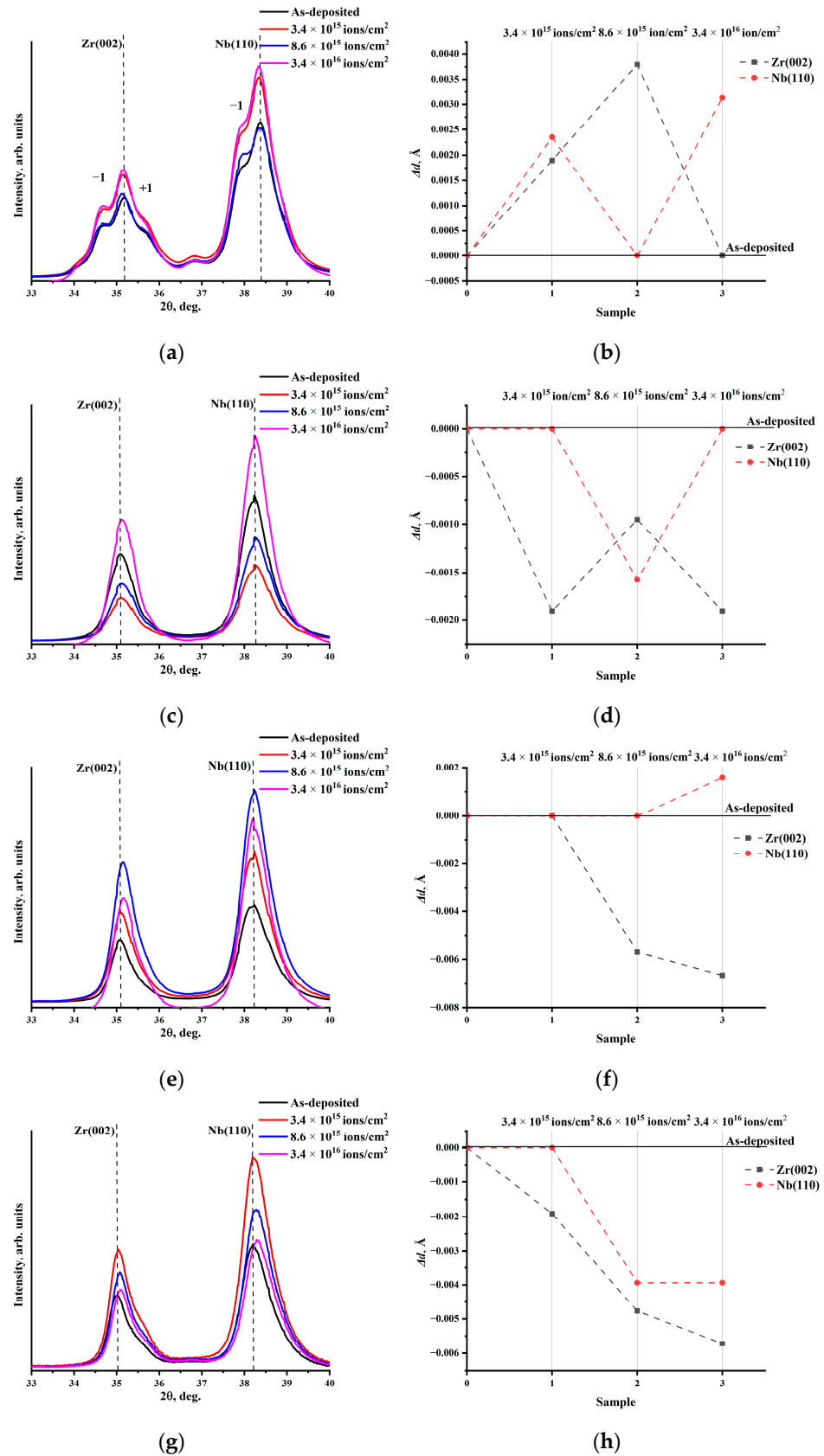


**Figure 5.** Figure 5. XRD patterns of as-deposited and proton-irradiated Zr/Nb NMCs: Zr10/Nb10 (a), Zr25/Nb25 (c), Zr50/Nb50 (e) and Zr100/Nb100 (g) samples and corresponding changes of d-spacing related to proton irradiation (b,d,f,h).

The obtained data confirm the results of the TEM studies. The structure of the as-deposited metallic multilayers is represented by Zr (002) and Nb (110) diffraction peaks (Figure 5a,c,e,g); additionally, satellites of major peaks are observed for Zr10/Nb10 samples (labeled as +1 and −1) (Figure 5a). Irradiation with protons at the indicated fluences does not cause significant structural changes in Zr/Nb NMCs. The shape of the reflections for all types of coating and at all irradiation fluences remains the same; the crystallographic orientation of the Zr and Nb layers does not change. From the presented results of the X-ray diffraction study, it can be seen that, due to proton irradiation, shifts in diffraction peaks and changes in interplanar distance (d-spacing) occur. The d-spacings for as-deposited Zr25/Nb25, Zr50/Nb50 and Zr100/Nb100 were 2.554 Å for the Zr layers and 2.351 Å for the Nb layers; at the same time, Zr10/Nb10 showed slightly lower d-spacing (2.549 Å for Zr layers, 2.342 Å for Nb layers) as evidenced from the position of the major diffraction peak. The changes in d-spacing are not uniform and differ for different coating thicknesses, layer material (Zr or Nb) and irradiation fluence. For Zr10/Nb10, there is an increase in the interplanar distance for the Zr and Nb layers relative to the as-deposited NMCs, whereas, relative to each other, an opposite trend in the d-spacing change can be observed for the  $8.6 \times 10^{15}$  and  $3.4 \times 10^{16}$  ions/cm<sup>2</sup> fluences (Figure 5b). This can be related to mechanical stresses with different signs (compressive and tensile) arising in the Zr and Nb layers [14] during irradiation. The same is observed for Zr25/Nb25, except that compared to the as-deposited samples, irradiated Zr/Nb NMCs showed a decrease in interplanar distance (Figure 5d). Zr25/Nb25 demonstrated the lowest d-spacing change of the NMCs presented in this study. For Zr50/Nb50 and Zr100/Nb100, the d-spacing change is more pronounced and a fluence-dependent trend can be observed (Figure 5f,h). In all types of Zr/Nb NMC, Zr layers are more vulnerable to proton irradiation, due to crystal structure and higher radiation damageability [19]. The nanohardnesses of as-deposited and proton-irradiated Zr/Nb NMCs are shown in Table 1.

**Table 1.** The nanohardness of as-deposited and proton-irradiated Zr/Nb nanoscale multilayer coatings (NMCs).

Individual Layer Thicknesses, nm	As-Deposited Zr/Nb NMCs	The Fluences of Irradiation, ions/cm <sup>2</sup>		
		$3.4 \times 10^{15}$	$8.6 \times 10^{15}$	$3.4 \times 10^{16}$
Nanohardness, ±20 HV				
10	1150 [11]	830 [11]	810	800
25	1050 [11]	650 [11]	700	740
50	930 [11]	650 [11]	650	670
100	600 [11]	640 [11]	800	780

After proton irradiation with a fluence of  $3.4 \times 10^{15}$  ions/cm<sup>2</sup>, the values of nanohardness for Zr10/Nb10 and Zr50/Nb50 NMCs decrease by 32% and 25%, respectively. A further increase in the fluence (up to  $3.4 \times 10^{16}$  ions/cm<sup>2</sup>) does not lead to a change in the nanohardness of the samples, whereas, for Zr25/Nb25 samples after irradiation with  $3.4 \times 10^{15}$  ions/cm<sup>2</sup> fluence, the nanohardness decreases by 30%. However, with a further increase in the fluence, a rise in nanohardness is observed. After irradiation with a fluence of  $3.4 \times 10^{15}$  ions/cm<sup>2</sup>, there is practically no change in the nanohardness of Zr100/Nb100 samples. With a growth in fluence to  $8.6 \times 10^{15}$ , an increase in nanohardness is observed, but a further rise in fluence (to  $3.4 \times 10^{16}$ ) does not lead to change in nanohardness.

The combined experimental data obtained allowed the characterization of the evolution of the microstructure and properties of Zr/Nb NMCs as a function of the proton irradiation fluence. For Zr10/Nb10 and Zr25/Nb25, increasing the proton irradiation fluence from  $3.4 \times 10^{15}$  to  $3.4 \times 10^{16}$  ions/cm<sup>2</sup> enhances the partial amorphization of the interfaces and causes a coherence change (incoherent to semicoherent) in the proton deposition region (up to ~130 nm). The embedded H atoms are unevenly distributed in this region, causing mechanical stresses of different signs (compressive and tensile)

in the Zr and Nb layers and insignificant fluctuations in the interplanar distance. These microstructural changes mainly have a negative effect on the nanohardness, which tends to increase with irradiation fluence, and have no effect on the positron annihilation characteristics, which would indicate the formation of radiation defects. The microstructure of all internal interfaces (300–1000 nm) of all proton-irradiated Zr/Nb NMCs remains unchanged regardless of the thickness of the individual layers.

The stability of the interfaces in the irradiated region is much better for NMC Zr50/Nb50. The variation in interplanar distance with increasing fluence is more pronounced for Zr50/Nb50, but the other microstructural characteristics and properties are virtually unchanged with increasing proton irradiation fluence. The interfaces persist as incoherent and there is no substantial radiation damage or material deterioration in the nanohardness, DBS and H profiles. For NMC Zr100/Nb100, the microstructural characteristics of the interfaces and the H profile are also preserved with increasing proton irradiation fluence, but there is an amplification of nanohardness and significant changes in the DBS profile. This indicates the accumulation of radiation defects and the formation of hydrogen-vacancy complexes in the irradiation area. When the irradiation area is comparable to the thickness of a single layer, energy and defect dissipation do not occur in NMCs because only the outer layer is active.

#### 4. Conclusions

The study of the effect of proton irradiation fluence on the microstructure, defects and nanohardness of Zr/Nb nanoscale multilayer coatings (NMCs) showed that the following:

1. Increasing the irradiation fluence from  $3.4 \times 10^{15}$  to  $3.4 \times 10^{16}$  ions/cm<sup>2</sup> leads to a partial destruction of the interfaces of Zr/Nb NMCs with layer thicknesses of 10–25 nm, which become semicoherent. This apparently contributes to vigorous proton implantation, whereas the irregular H accumulation at the interfaces is preserved.
2. The proton irradiation fluence increases do not lead to a noticeable deterioration in the microstructure and properties of Zr/Nb NMCs with 50 nm layer thicknesses. The microstructure is also preserved with increasing proton irradiation fluence for Zr100/Nb100, but there is an accumulation of hydrogen-vacancy complexes in the ion precipitation zone, which negatively affects the nanohardness.
3. The enhanced proton deposition at the interfaces of the Zr/Nb NMCs, as a result of the increasing radiation fluence, causes a change in the depth profile of the DBS parameters but does not reveal an intense accumulation of primary radiation defects for all NMCs with a layer thickness less than 100 nm. Positrons are predominantly annihilated in reduced electron density areas at interfaces near zirconium atoms before and after proton irradiation.

The kinetics of changes in the mechanical properties and microstructure of Zr/Nb NMCs with increasing proton irradiation fluence demonstrate the enhanced radiation tolerance of these coatings and actualize their further study at higher damaging doses. However, they also reveal several peculiarities and limitations related to the localization of radiation damage and the thickness of individual layers. Systems with thinner layers can absorb defects more effectively, due to the high number of interfaces, but are more susceptible to microstructural degradation. Interfaces of systems with thicker layers are less vulnerable to radiation degradation, but the efficiency is less and depends on the localization of the embedded ions. Radiation tolerance is diminished when the area of radiation damage is comparable to the thickness of the layer. The effect of temperature during irradiation or subsequent thermal exposure is the subject of further investigation.

**Author Contributions:** R.L. conducted the organization of the experimental procedure and preparation of the manuscript. E.S. carried out the microstructure analysis using TEM. N.P. performed and analyzed the results of the mechanical tests. A.L. examined the samples using the GD-OES method. D.K. and E.K. provided the SRIM calculations and the XRD analysis. A.D., A.S. and O.O. performed proton irradiation and layer-by-layer analysis using positron spectroscopy methods. V.U. carried out a comprehensive analysis of the received data and prepared the manuscript for publication. All authors have read and agreed to the published version of the manuscript.

**Funding:** This work was funded by the Russian Science Foundation, research project No. 20-79-10343.

**Data Availability Statement:** Not applicable.

**Acknowledgments:** The TEM and STEM research was carried out using the equipment of the CSU NMNT TPU, supported by the RF MES project No. 075-15-2021-710.

**Conflicts of Interest:** The authors declare no conflict of interest.

## References

1. Parihar, R.S.; Setti, S.G.; Sahu, R.K. Recent Advances in the Manufacturing Processes of Functionally Graded Materials: A Review. *Sci. Eng. Compos. Mater.* **2018**, *25*, 309–336. [[CrossRef](#)]
2. Li, Y.; Feng, Z.; Hao, L.; Huang, L.; Xin, C.; Wang, Y.; Bilotti, E.; Essa, K.; Zhang, H.; Li, Z.; et al. A Review on Functionally Graded Materials and Structures via Additive Manufacturing: From Multi-Scale Design to Versatile Functional Properties. *Adv. Mater. Technol.* **2020**, *5*, 1900981. [[CrossRef](#)]
3. Metalnikov, P.; Eliezer, D.; Ben-Hamu, G. Hydrogen Trapping in Additive Manufactured Ti–6Al–4V Alloy. *Mater. Sci. Eng. A* **2021**, *811*, 141050. [[CrossRef](#)]
4. Navi, N.U.; Tenenbaum, J.; Sabatani, E.; Kimmel, G.; Ben David, R.; Rosen, B.A.; Barkay, Z.; Ezersky, V.; Tiferet, E.; Ganor, Y.I.; et al. Hydrogen Effects on Electrochemically Charged Additive Manufactured by Electron Beam Melting (EBM) and Wrought Ti–6Al–4V Alloys. *Int. J. Hydrogen Energy* **2020**, *45*, 25523–25540. [[CrossRef](#)]
5. Svetlizky, D.; Das, M.; Zheng, B.; Vyatskikh, A.L.; Bose, S.; Bandyopadhyay, A.; Schoenung, J.M.; Lavernia, E.J.; Eliaz, N. Directed Energy Deposition (DED) Additive Manufacturing: Physical Characteristics, Defects, Challenges and Applications. *Mater. Today* **2021**, *49*, 271–295. [[CrossRef](#)]
6. Doğu, M.N.; Esen, Z.; Davut, K.; Tan, E.; Gümüş, B.; Dericioglu, A.F. Microstructural and Texture Evolution during Thermo-Hydrogen Processing of Ti6Al4V Alloys Produced by Electron Beam Melting. *Mater. Charact.* **2020**, *168*, 110549. [[CrossRef](#)]
7. Callisti, M.; Karlik, M.; Polcar, T. Competing Mechanisms on the Strength of Ion-Irradiated Zr/Nb Nanoscale Multilayers: Interface Strength versus Radiation Hardening. *Scr. Mater.* **2018**, *152*, 31–35. [[CrossRef](#)]
8. Sen, H.S.; Polcar, T. Vacancy-Interface-Helium Interaction in Zr-Nb Multi-Layer System: A First-Principles Study. *J. Nucl. Mater.* **2019**, *518*, 11–20. [[CrossRef](#)]
9. Daghbouj, N.; Callisti, M.; Sen, H.S.; Karlik, M.; Čech, J.; Vronka, M.; Havránek, V.; Čapek, J.; Minárik, P.; Bábó, P.; et al. Interphase Boundary Layer-Dominated Strain Mechanisms in Cu+ Implanted Zr-Nb Nanoscale Multilayers. *Acta Mater.* **2021**, *202*, 317–330. [[CrossRef](#)]
10. Daghbouj, N.; Sen, H.S.; Čížek, J.; Lorinčík, J.; Karlik, M.; Callisti, M.; Čech, J.; Havránek, V.; Li, B.; Krsjak, V.; et al. Characterizing Heavy Ions-Irradiated Zr/Nb: Structure and Mechanical Properties. *Mater. Des.* **2022**, *219*, 110732. [[CrossRef](#)]
11. Laptev, R.; Stepanova, E.; Pushilina, N.; Svyatkin, L.; Krotkevich, D.; Lomygin, A.; Ognev, S.; Siemek, K.; Doroshkevich, A.; Uglov, V. Distribution of Hydrogen and Defects in the Zr/Nb Nanoscale Multilayer Coatings after Proton Irradiation. *Materials* **2022**, *15*, 3332. [[CrossRef](#)] [[PubMed](#)]
12. Laptev, R.; Svyatkin, L.; Krotkevich, D.; Stepanova, E.; Pushilina, N.; Lomygin, A.; Ognev, S.; Siemek, K.; Uglov, V. First-Principles Calculations and Experimental Study of H+-Irradiated Zr/Nb Nanoscale Multilayer System. *Metals* **2021**, *11*, 627. [[CrossRef](#)]
13. Laptev, R.; Lomygin, A.; Krotkevich, D.; Syrtanov, M.; Kashkarov, E.; Bordulev, Y.; Siemek, K.; Kobets, A. Effect of Proton Irradiation on the Defect Evolution of Zr/Nb Nanoscale Multilayers. *Metals* **2020**, *10*, 535. [[CrossRef](#)]
14. Laptev, R.; Stepanova, E.; Pushilina, N.; Kashkarov, E.; Krotkevich, D.; Lomygin, A.; Sidorin, A.; Orlov, O.; Uglov, V. The Microstructure of Zr/Nb Nanoscale Multilayer Coatings Irradiated with Helium Ions. *Coatings* **2023**, *13*, 193. [[CrossRef](#)]
15. Shulepov, I.; Lomygin, A.; Roman, L.; Kashkarov, E.; Syrtanov, M. Correction of the Distribution Profiles of the Intensities of Elements Considering the Uneven Dispersion of the Glow-Discharge Optical Emission Spectrometer for Multilayer Coatings Analysis. In Proceedings of the 2020 7th International Congress on Energy Fluxes and Radiation Effects (EFRE), Tomsk, Russia, 14–26 September 2020. [[CrossRef](#)]
16. Kuznetsov, P.V.; Mironov, Y.P.; Tolmachev, A.I.; Rakhmatulina, T.V.; Bordulev, Y.S.; Laptev, R.S.; Lider, A.M.; Mikhailov, A.A.; Korznikov, A.V. Positron Annihilation Spectroscopy of Vacancy-Type Defects Hierarchy in Submicrocrystalline Nickel during Annealing. In Proceedings of the International Conference On Physical Mesomechanics of Multilevel Systems 2014, Tomsk, Russia, 14–26 September 2014. [[CrossRef](#)]
17. Bordulev, I.; Kudiiarov, V.; Svyatkin, L.; Syrtanov, M.; Stepanova, E.; Čížek, J.; Vlček, M.; Li, K.; Laptev, R.; Lider, A. Positron Annihilation Spectroscopy Study of Defects in Hydrogen Loaded Zr-1Nb Alloy. *J. Alloys Compd.* **2019**, *798*, 685–694. [[CrossRef](#)]

18. Kuznetsov, P.V.; Mironov, Y.P.; Tolmachev, A.I.; Bordulev, Y.S.; Laptev, R.S.; Lider, A.M.; Korznikov, A.V. Positron Spectroscopy of Defects in Submicrocrystalline Nickel after Low-Temperature Annealing. *Phys. Solid State* **2015**, *57*, 219–228. [[CrossRef](#)]
19. Konobeyev, A.Y.; Fischer, U.; Korovin, Y.A.; Simakov, S.P. Evaluation of Effective Threshold Displacement Energies and Other Data Required for the Calculation of Advanced Atomic Displacement Cross-Sections. *Nucl. Energy Technol.* **2017**, *3*, 169–175. [[CrossRef](#)]

**Disclaimer/Publisher’s Note:** The statements, opinions and data contained in all publications are solely those of the individual author(s) and contributor(s) and not of MDPI and/or the editor(s). MDPI and/or the editor(s) disclaim responsibility for any injury to people or property resulting from any ideas, methods, instructions or products referred to in the content.